

Available online at www.sciencedirect.com

Thin Solid Films xx (2006) xxx–xxx

www.elsevier.com/locate/tsf

Laser damage resistance of silica thin films deposited by Electron Beam Deposition, Ion Assisted Deposition, Reactive Low Voltage Ion Plating and Dual Ion Beam Sputtering

L. Gallais*, H. Krol, J.Y. Natoli, M. Commandré, M. Cathelinaud,
L. Roussel, M. Lequime, C. Amra

*Institut Fresnel (UMR CNRS 6133) - Université Paul Cezanne - Université de Provence - Ecole Centrale Marseille,
Domaine Universitaire de St Jérôme - 13397 Marseille Cedex 20 - France*

Received 24 April 2006; received in revised form 27 September 2006; accepted 6 October 2006

Abstract

The laser damage resistance of optical coatings is a key point for a large number of applications. The aim of this work is to test and analyze the laser damage resistance of a thin film material commonly used for high power applications (SiO_2) and deposited with different techniques: Electron Beam Deposition, Ion Assisted Deposition, Low Voltage Reactive Ion Plating and Dual Ion Beam Sputtering. The laser damage thresholds of these coatings were determined at 1064 nm and 355 nm using nanosecond pulsed YAG lasers, with a 1-on-1 test procedure. The results are then compared and discussed: we found different behaviours that we link to laser damage initiators of different nature and densities. The dense thin films (obtained with ion assistance) were found to be highly resistant to laser damage.

© 2006 Elsevier B.V. All rights reserved.

Keywords: Laser damage; Optical coatings; Silicon oxide; Evaporation; Sputtering

1. Introduction

Producing laser damage resistant optical coatings has a considerable interest for high power laser applications. However, improving this resistance is often a difficult task because of the large number of parameters of the manufacturing processes than can affect the properties of the resulting layers and modify the laser damage threshold. For instance the substrate temperature and starting source material (oxide or metal), the parameters of plasma arc and source, the deposition rate, the gas partial pressures [1–6] ... play a key role. Then high laser damage threshold coatings can be fabricated when the mechanisms and sources of damage are well understood. Laser damage resistance of coatings has been the subject of

many studies (see for example the review articles [7–9] on this subject). But deposition technologies have evolved and processes have been improved, then new studies on this subject are required. In addition it is often difficult to compare laser damage performances if the measurements are not made in exactly the same conditions. Indeed the damage threshold can be linked to many factors such as the test procedure, the spot size, the wavelength, the pulse duration, the number of shots... (see for instance the results of the Round-Robin experiment in Ref [10]).

So in the aim of producing high laser damage threshold coatings, we propose in this paper to make a comparative study of the laser damage resistance of identical coatings deposited through various techniques. We chose in a first stage to study silica thin films, which is one of the most used oxide material for the manufacture of interference multilayer coatings, and which is also known as a very high laser damage threshold material [7]. We used the different processes available at the Institut Fresnel, to produce these thin films in well known conditions.

* Corresponding author.

E-mail address: laurent.gallais@fresnel.fr (L. Gallais).

URL: www.fresnel.fr (L. Gallais).

2. Materials and methods

2.1. Samples description and preparation

The influence of the substrate features is important and can ultimately limit the thresholds for a given coating [1,8]. We have chosen Herasil glasses specially polished for high power applications, and coming from the same batch. To clean these substrates we used an automatic aqueous cleaning procedure, involving ultrasonic immersion and detergents followed by de-ionized water rinsing and drying.

To check the cleaning efficiency for all the samples, a bare silica reference sample was associated to each batch. These samples have been inspected after cleaning through a dark field microscope and images were analyzed with a defect counting software. The procedure is the following: 5 images are randomly taken in dark field mode on the sample (field of view is $260 \times 195 \mu\text{m}^2$) and turned into binary images, the software then counts the number of white dots and gives the density of defects on the tested surface. This procedure was also applied to each thin film sample after deposition. This method allows the observation of micronic scattering defects and gives a statistic information on the cleanliness before and after deposition. The method is used for comparison between samples, then the sensitivity limit has not been measured. The results are given in Section 3.

To investigate the influence of the film thickness in the laser damage resistance, we chose to deposit coatings with two different thicknesses: 200 nm and 1000 nm (mechanical thickness). Two layers were made for each thickness to check the reproducibility of the process. The optical thickness of the layer is not here a relevant parameter, because of the very low refractive index difference between the substrate and the layer. At the end, 18 thin film samples were produced for this study, and 5 bare reference substrates corresponding to the 5 cleaning batches (one for each deposition technique), were used.

2.2. Deposition techniques

For the thin films deposited by Electron Beam Deposition (EBD) and Reactive Low Voltage Ion Plating (RLVIP), the equipment used was a Balzers BAP 800 Ion-Plating system, that is described precisely in Ref [11]. The chamber contains two crucibles heated by electron-beam guns and a source of Argon plasma that is used to obtain the densification of the layer (ion plating). In the absence of the use of this source, the layers are thus obtained through standard EBD process. The rate of evaporation (0.8 nm/s) during the deposition is controlled by a quartz-crystal monitor and the optical thicknesses of the layers are moreover controlled by an *in situ* optical monitoring system. The material used for these two processes was silicon with 99.999% purity, deposited under an oxygen partial pressure (respectively 9×10^{-2} Pa for EBD and 9.5×10^{-2} Pa for RLVIP).

The Ion Assisted Deposition (IAD) was made with a Balzers BAK 750 system, under the assistance of an Argon Ion beam. Again, the chamber contains two electron beam guns, a quartz crystal thickness controller, and an *in situ* optical monitoring

system. The deposition rate was set between 0.2 and 0.6 nm/s. The ultimate pressure was 3×10^{-5} Pa, and reached 3×10^{-2} Pa during the deposition phase (partial oxygen pressure). The material source was silica.

A Teer Coating equipment was used for the Dual Ion Beam Sputtering process (DIBS). With this technique, a first ion source is used for sputtering a plane target (here in silicon), and a second ion source is directed towards the substrates for providing argon ions, whose energy is used to compact the layer material. As before, the vacuum chamber is equipped with quartz-thickness-controller and *in situ* optical monitoring. The deposition rate was set between 0.1 and 0.2 nm/s. The ultimate pressure was 7×10^{-5} Pa, and reached 3×10^{-2} Pa during the deposition phase.

For all the deposition processes, the substrates are not heated by external means (like resistive heaters or lamps) and the final temperature is directly connected with the nature of the process: 250 °C for EBD, 150 °C for RLVIP, 50 °C for DIBS and IAD.

2.3. Laser damage measurements

The test apparatus used for laser damage testing has been described in detail in another paper [12], and only a brief description is given here. We used a first YAG laser beam with 1.064- μm wavelength and 5-ns effective pulse duration. The beam was focused down to a spot diameter of 12- μm on the sample. A second frequency-tripled YAG laser was used for 355 nm testing (spot diameter of 8- μm and 6 ns effective pulse duration). The sample was observed by an *in situ* optical microscope (magnification from $\times 50$ to $\times 500$), which ensures real-time observation and recording of the irradiated zone. Any image modification after shot is our damage criterium (micronic damage can be detected).

Using this apparatus, we measured laser damage probability curves with the 1-on-1 test procedure [13]. We recall that these curves are obtained by counting the number of damaged regions at each fluence F , which allows to estimate the damage probability $P(F)$. We adopted a very refined test procedure in comparison with the ISO norm [13]: a first plot is made by

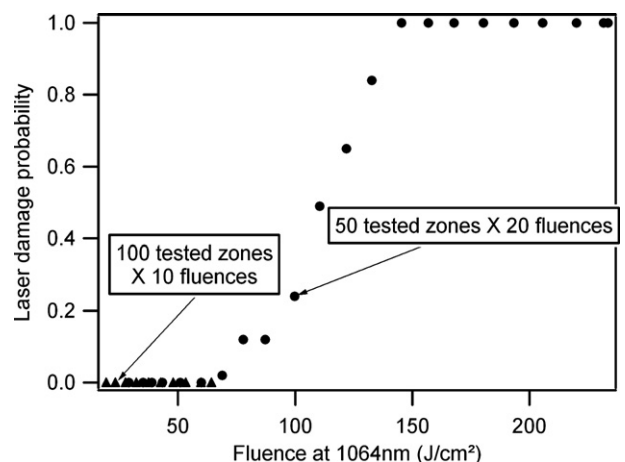


Fig. 1. Example of a laser damage measurement on a bare silica substrate (Herasil).

Table 1
Density of visible defects with Dark Field Microscopy ($\times 200$) on the samples, after cleaning

Sample number	1	2	3
Uncleaned bare substrate	460/mm ²	–	–
Cleaned bare substrates	5/mm ²	35/mm ²	10/mm ²
DIBS (200 nm)	10/mm ²	15/mm ²	–
DIBS (1000 nm)	15/mm ²	5/mm ²	–
IAD (200 nm)	10/mm ²	30/mm ²	–
IAD (1000 nm)	265/mm ²	170/mm ²	–
RLVIP (200 nm)	100/mm ²	65/mm ²	–
RLVIP (1000 nm)	105/mm ²	135/mm ²	–

The ‘uncleaned bare substrate’ is a sample measured directly after being supplied. The 3 bare substrates were used as reference samples: the substrates used for the DIBS samples were cleaned together with the bare substrate 1, the IAD substrates were cleaned with the bare substrate 3 and the RLVIP samples with the substrate 2. The EBD samples and their reference samples have not been tested before the damage tests.

testing 50 points for each energy (with 20 different energies), then a “zoom” is done on the low part of the curve, in order to determine with a great accuracy the laser damage threshold of the sample. This second test is done by testing 100 points for each energy (with 10 different energies). At the end, each laser damage measurement is the result of a statistic made on 2000

different measurement points for the corresponding sample. An example of result is shown on Fig. 1 for the case of a bare silica substrate (Herasil) as used in this study.

3. Results

3.1. Thin films surface quality

As explained in Section 2, all the samples were checked under dark field microscopy and a software was used to automatically count the number of visible defects on the coatings and substrates. The results are summarized in Table 1.

A good cleaning with our procedure results in less than 10 defects/mm² (visible in dark field microscopy with $\times 500$ magnification), which is the case for the reference substrate 1 and 3. As concerns the substrate 2, it exhibits however a higher defect density. The DIBS samples (cleaned with substrate 1) have a very good quality since the defect density is the same as the substrate. The Ion Plating process deposition has introduced some defects on the RLVIP samples (around 100 defects/mm²) compared to the reference sample 2: ten times the initial density. For the IAD samples, a notable difference exists between 200 nm samples and 1000 nm samples. Whereas 200 nm samples are clean compared to their reference substrate (3), the

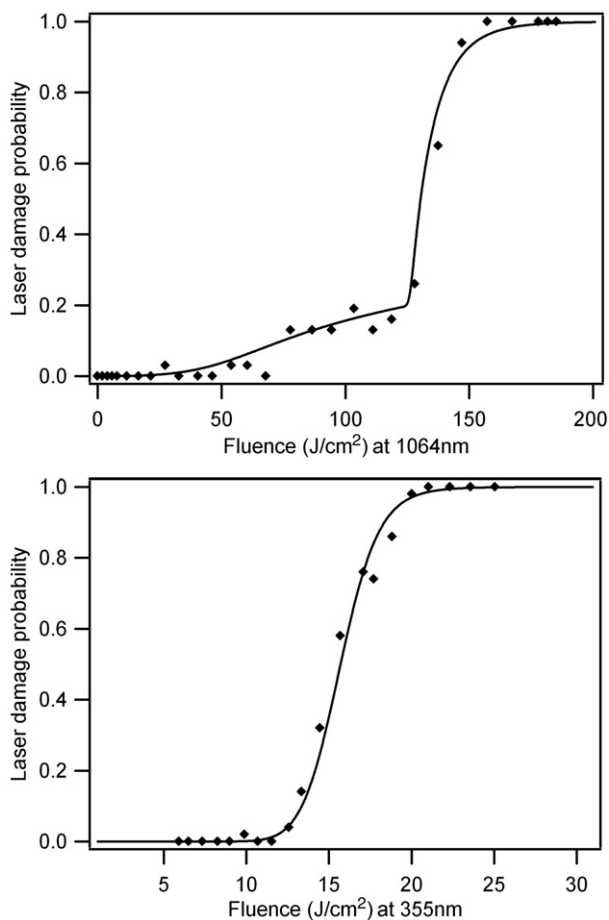


Fig. 2. Measurement and fit with the model of laser damage probability curves of a DIBS thin film tested at 1064 and 355 nm.

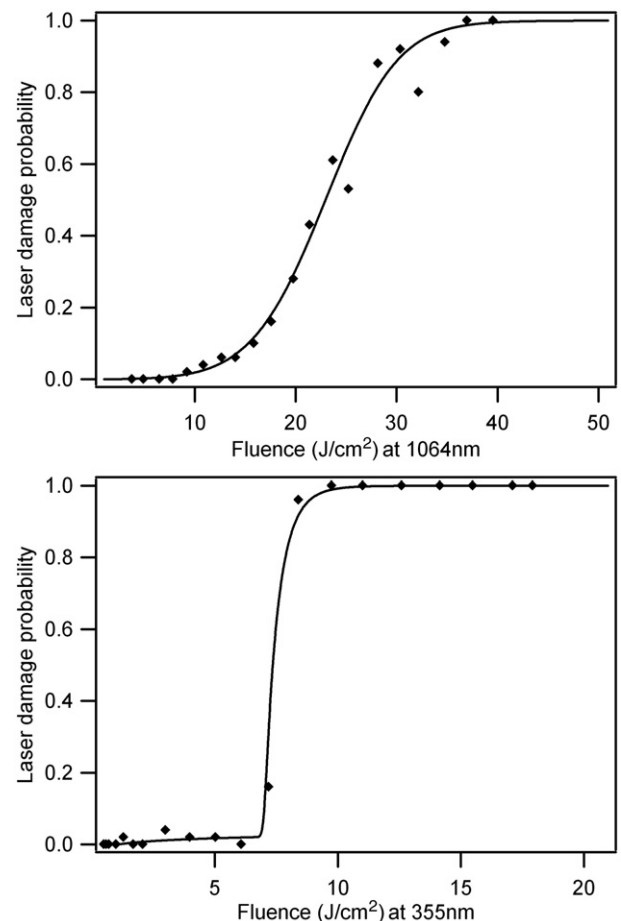


Fig. 3. EBD thin film tested at 1064 and 355 nm.

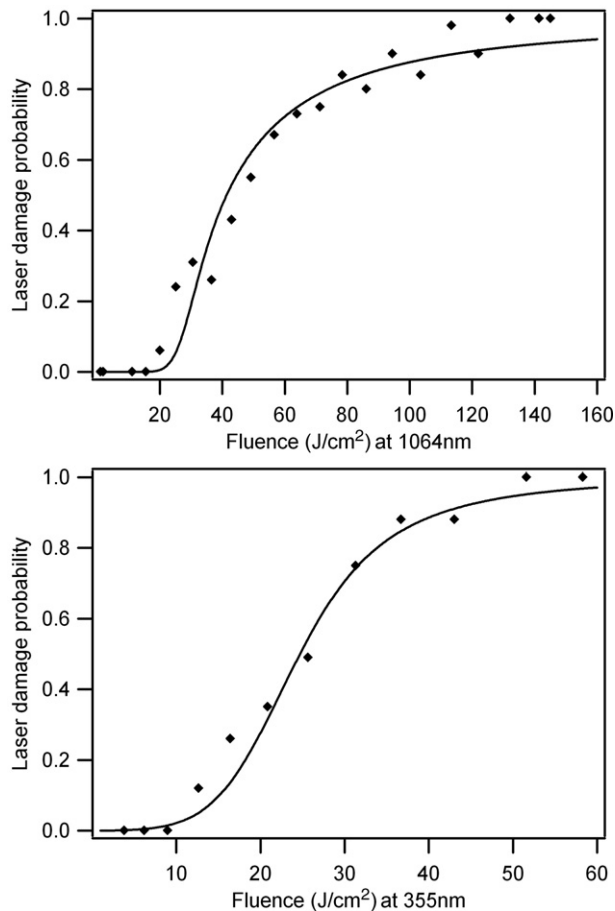


Fig. 4. RLVIP thin film tested at 1064 and 355 nm.

others (1000 nm) exhibit a very high density of defects even if the causes of these phenomena are not clear.

3.2. IR and UV laser damage measurements

Laser damage measurements were done on each sample with the procedure described in Section 2.3. Not all the curves are given in this paper, we have plotted only representative curves for each kind of samples and wavelength on Figs. 2, 3, 4 and 5.

Obviously, each kind of sample exhibits a different behaviour as regards the curve shape and the threshold. These shape and threshold are linked to the initiator characteristics (density, nature,...). We can obtain data on these initiators by fitting the experimental curves with an adapted model as the one described in Ref [14]. This has been done on each curve in this study (curve in full line in the figures). A very good agreement has been obtained between our data and the model, evidencing different randomly distributed initiators on each sample. The curves are then discussed with the help of this statistical model.

- On the DIBS samples at 1064 nm, two types of laser damage precursors are observed: one with a threshold of $35 \pm 5 \text{ J/cm}^2$ and density of $600 \pm 200/\text{mm}^2$ and the other of $110 \pm 20 \text{ J/cm}^2$, with a higher density of $5 \pm 2 \times 10^4/\text{cm}^2$. We observe no difference in the threshold or number of the precursors between the samples of different thicknesses.

At 355 nm, different layers were made (referenced as DIBS5 and DIBS6) with an optimized procedure for this wavelength (slower deposition speed) and a thickness of 200 nm. These layers have a threshold of 9 J/cm^2 and one kind of precursor is detected.

- As concerns the EBD samples, we observe at 1064 nm one kind of precursor with a threshold of $12 \pm 2 \text{ J/cm}^2$ and with a density depending on the thin film thickness: $1 \pm .5 \times 10^4/\text{mm}^2$ for the 200 nm samples and $5 \pm 1 \times 10^4/\text{mm}^2$ for the 1000 nm samples. From these results it comes out that the number of defects for this kind of technique is dependent on the film thickness (or the deposition time). It is a good indication that they must be embedded inside the bulk of the film all along the deposition process.
- At 355 nm two kinds of initiators appear: the first appears at $4 \pm 1 \text{ J/cm}^2$ with a density lower than 40 defects/mm^2 , and the other at $6 \pm 1 \text{ J/cm}^2$. However we do not observe in this case any clear dependence with the film thickness.
- On the RLVIP samples we detect one kind of precursors on the 200 nm thickness samples and two kinds on the 1000 nm samples at 1064 nm. The corresponding threshold and densities for the 200 nm samples are $20 \pm 2 \text{ J/cm}^2$, $7 \times 10^3/\text{mm}^2$. The 1000 nm samples were found to be less resistant to laser damage, with defects having a threshold of $11 \pm 1 \text{ J/cm}^2$ (density = $300/\text{mm}^2$) and $40 \pm 5 \text{ J/cm}^2$ (density = $2 \times 10^4/\text{mm}^2$).

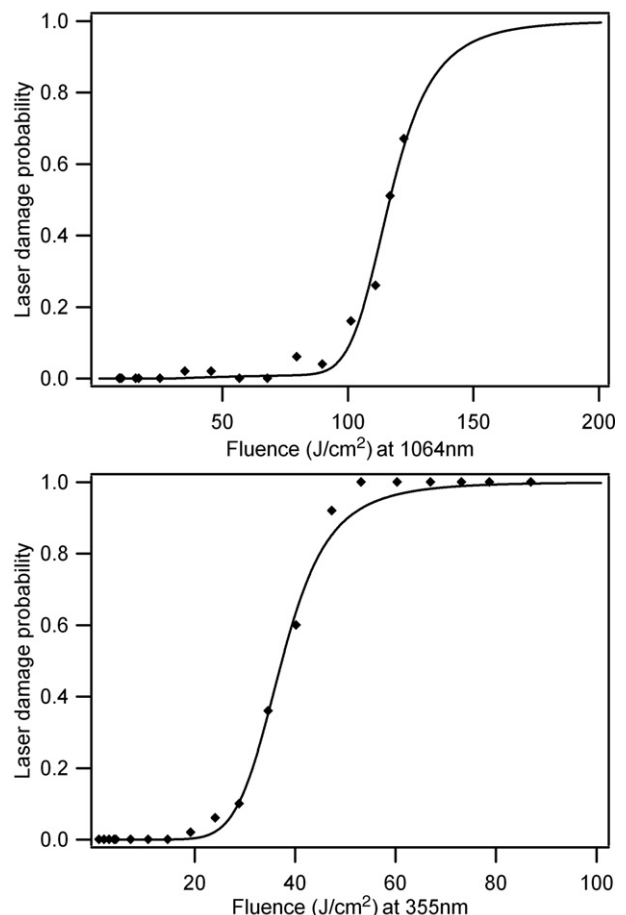


Fig. 5. IAD thin film tested at 1064 and 355 nm.

We can note that if we do not see two kinds of precursors for the 200 nm samples, it could be due to the limitation of the technique: defect densities less than few $10^4/\text{mm}^2$ are not detected with our setup. Nevertheless, for this deposition technique, the threshold variation with thickness suggests a production of these defects during the deposition process, as for the EBD technique (we can note that the same equipment and material source were used).

In the UV the same defects (threshold of $10 \pm 1 \text{ J/cm}^2$ and density of $9 \times 10^3/\text{mm}^2$) were found on all the samples. In the case of the 1000 nm layers, it appears that the threshold in the UV is slightly better than in the infrared (see the summary of results in Table 2), this special situation implies that the initiators and mechanisms are different, which is supported by the fact that there are two orders of magnitude between the density of defects found in the infrared and the UV.

- The IAD samples exhibit the same behaviour at 1064 nm: two kinds of defects, one with a threshold of $100 \pm 10 \text{ J/cm}^2$ and a density of $3 \times 10^4/\text{mm}^2$ the other with a lower density ($400/\text{mm}^2$) and a threshold of $30 \pm 3 \text{ J/cm}^2$. However in the UV, a difference appears between samples of 200 nm and 1000 nm due to the defects with low density that appear in the thickest layers. This difference in thresholds is related to an increase of the visible number of defects by dark field microscopy (see Table 1) and could be linked to contamination of the layer during or after deposition. In this case the defects involved are not limiting the 1064 nm LIDT. We can

Table 2
Summary of laser damage thresholds and laser damage precursor densities found on the different samples

	LIDT		Damage initiators	
	At 1064 nm	At 1064 nm	At 355 nm	At 355 nm
Uncleaned substrate	28 J/cm ²	$1 \times 10^6/\text{mm}^2$	22 J/cm ²	$2 \times 10^4/\text{mm}^2$
Bare substrate 1	73 J/cm ²	$2 \times 10^4/\text{mm}^2$	31 J/cm ²	$2 \times 10^4/\text{mm}^2$
Bare substrate 2	70 J/cm ²	$2 \times 10^4/\text{mm}^2$	20 J/cm ²	$2 \times 10^4/\text{mm}^2$
Bare substrate 3	67 J/cm ²	$3 \times 10^4/\text{mm}^2$	25 J/cm ²	$5 \times 10^4/\text{mm}^2$
Bare substrate 4	77 J/cm ²	$5 \times 10^4/\text{mm}^2$	22 J/cm ²	$4 \times 10^4/\text{mm}^2$
DIBS 1 (200 nm)	30 J/cm ²	$1 \times 10^3/\text{mm}^2$	–	–
DIBS 2 (200 nm)	38 J/cm ²	$5 \times 10^2/\text{mm}^2$	–	–
DIBS 3 (1000 nm)	40 J/cm ²	$7 \times 10^2/\text{mm}^2$	–	–
DIBS 4 (1000 nm)	34 J/cm ²	$6 \times 10^2/\text{mm}^2$	–	–
DIBS 5 (200 nm)	–	–	9 J/cm ²	$8 \times 10^4/\text{mm}^2$
DIBS 6 (200 nm)	–	–	8 J/cm ²	$2 \times 10^4/\text{mm}^2$
RLVIP 1 (200 nm)	20 J/cm ²	$7 \times 10^3/\text{mm}^2$	9 J/cm ²	$2 \times 10^4/\text{mm}^2$
RLVIP 2 (200 nm)	18 J/cm ²	$1 \times 10^3/\text{mm}^2$	7 J/cm ²	$1.5 \times 10^4/\text{mm}^2$
RLVIP 1 (1000 nm)	12 J/cm ²	$3 \times 10^2/\text{mm}^2$	14 J/cm ²	$2 \times 10^4/\text{mm}^2$
RLVIP 2 (1000 nm)	12 J/cm ²	$3 \times 10^2/\text{mm}^2$	14 J/cm ²	$2 \times 10^4/\text{mm}^2$
IAD 1 (200 nm)	36 J/cm ²	40/mm ²	19 J/cm ²	$2 \times 10^2/\text{mm}^2$
IAD 2 (200 nm)	36 J/cm ²	40/mm ²	18 J/cm ²	$6 \times 10^2/\text{mm}^2$
IAD 1 (1000 nm)	–	–	11 J/cm ²	2/mm ²
IAD 2 (1000 nm)	34 J/cm ²	40/mm ²	10 J/cm ²	2/mm ²
EBD 1 (200 nm)	13 J/cm ²	$1.5 \times 10^4/\text{mm}^2$	5 J/cm ²	$6 \times 10^4/\text{mm}^2$
EBD 2 (200 nm)	14 J/cm ²	$1.5 \times 10^4/\text{mm}^2$	5 J/cm ²	$1 \times 10^4/\text{mm}^2$
EBD 1 (1000 nm)	13 J/cm ²	$4 \times 10^4/\text{mm}^2$	3 J/cm ²	$1 \times 10^2/\text{mm}^2$
EBD 2 (1000 nm)	9 J/cm ²	$6 \times 10^4/\text{mm}^2$	2.5 J/cm ²	$2 \times 10^2/\text{mm}^2$

In case of several kinds of precursors detected, only the values for the limiting one (lowest threshold) are given. The accuracy is $\pm 20\%$ for density, and $\pm 5\%$ for threshold.

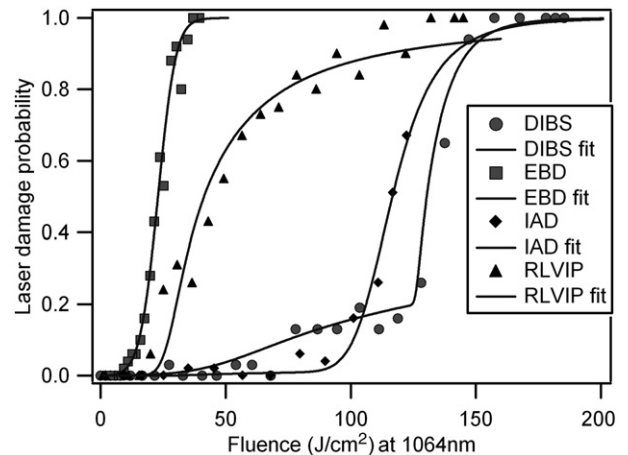


Fig. 6. Comparison of the laser damage probability curves at 1064 nm.

note however that these coatings have a very high laser damage threshold at 355 nm (the substrate value is almost reached for the 200 nm samples).

3.3. Summary of results

To compare the results, we have plotted on Figs. 6 and 7 a comparison of the curves given in the previous section. All the results (damage thresholds and defect densities) are summarized in Table 2. The results obtained on the bare substrates are also given: the publication of the results for a standard type of silica could be an efficient way to compare results from tests executed by different laboratories.

These results, useful for comparative study of the different technologies, should however be used with precaution for applications, since the measurements were made with a small spot size. Indeed, even if a high number of shots were applied for each energy, the total surface tested on the optic is in the order of 10^{-2} mm^2 , and in the case of tests with larger spot sizes, other kind of defects with lower densities could be involved, resulting in a lower threshold.

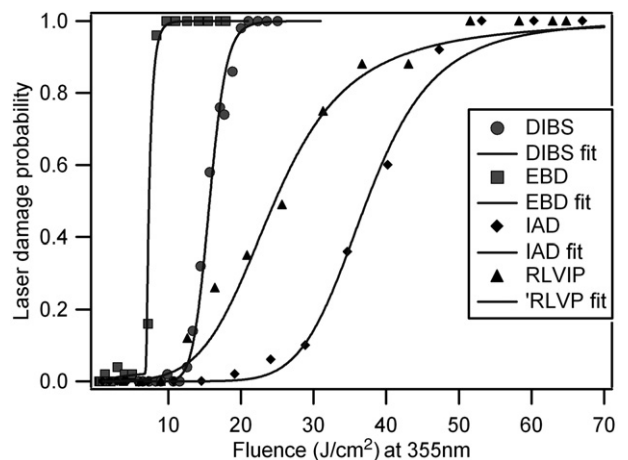


Fig. 7. Comparison of the laser damage probability curves at 355 nm.

4. Discussion

4.1. Initiation by micronic defects

It is commonly assumed that laser damage on coatings is linked to large defects, such as cracks, nodular structures, dirt, scratches,... or microscopic defects such as impurities, voids, grain boundaries,... which limit local laser damage resistance [15]. An evidence of the initiation by precursor can be found by examining the laser damage morphology, as shown in Fig. 8 where we can see typical laser damage morphologies on the EBD and DIBS samples. On the upper left image for instance, one can see two pits and a shallow print of the laser spot in the layer: on this area a damage has certainly been initiated by two precursors. The final aspect of the damage shows two deep pits that could correspond to the localization of laser damage initiators, and a shallow print of the laser spot in the layer (due to plasma burning). On the upper center image, the same process has occurred but with a precursor on the edge of the laser spot, which has not seen the maximum fluence of the spot. The upper right image shows the damage aspect with a higher fluence: delamination of the layer begins to occur. The same behaviour has been observed on all samples, with different diameters for the pits: 1–2 μm for the IAD and RLVIP techniques, less than 1 μm for EBD samples and less than few hundreds nanometers for the DIBS samples. The initiators and layer properties are certainly different, which could explain these differences, but in each case these precursors must have sub-micrometric scales to induce such small pits. The identification of these damage initiators is still an open problem today.

4.2. Influence of the deposition technique

High laser damage threshold is often reported in the literature for low density thin films, such as those obtained by Sol–Gel or Electron Beam Deposition [4,5,7,16–18], and different explanations have been given to explain this fact. For instance, by taking into account relatively large (well over 1 μm) absorbing inclusions embedded in the layer: during the irradiation, the inclusion is heated by absorption of the laser energy, and due to thermal expansion, pressure is applied on the film. This pressure

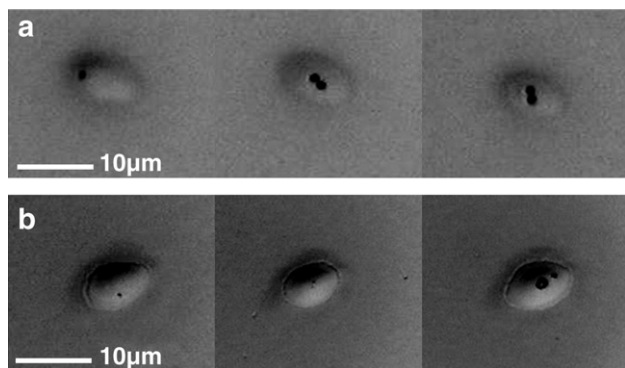


Fig. 8. 1064 nm laser damage morphologies observed by Nomarski microscopy on EBD (a) and DIBS (b) thin films.

could be dissipated when the film is porous [19], which could explain a better laser damage resistance for porous thin films. This argument however becomes less pertinent when the layers are free from micronic defects or if the laser damage mechanism is different from the one described above: for instance, as proposed by Papernov et al. [20], the defect can first absorb the laser energy, then the energy is transferred during the pulse from the heated defect to the surrounding matrix, causing the conversion of SiO_2 into an absorbing medium, which leads to a macroscopic damage if enough energy is deposited.

In our study, we observe that the dense layers (obtained with ion-assisted processes) exhibit a very good threshold in the infrared (DIBS) and the UV (IAD) compared with layers manufactured by classical EBD. In this case, the lack of ‘large’ absorbing defects causing damage by thermal expansion in the coating could be a first explanation (supported by the fact that pit diameters are micronic). In addition, for dense layers the thermal conductivity is larger than in the case of porous layers [21], and then in the case of a thermal process for the laser damage initiation, one should expect a larger threshold for the dense layer due to better heat dissipation [22] from the defect.

The possible adjustment of the oxygen partial pressure and ion energy to control the stoichiometry of the layers can have also a major influence on the laser damage threshold, as shown for instance by Hacker et al. [2] and Thielsch et al. [6]. This structural difference could explain the differences observed between the assisted deposition techniques in our study. Of course, further analysis is still required for more fundamental understanding.

In fact the improvement of the microstructure and stoichiometry using high energy techniques, combined with a low density of relatively small defects is the best way to improve the laser damage resistance. However the assisting-ion-beam energy parameters are very critical for the laser damage threshold, as shown for instance by the study of Alvisi et al. [23] on this subject.

Finally, the Dual Ion Beam Sputtering technique appears to be a promising technique for the production of high laser damage threshold coatings, since it also leads to very good mechanical, structural and optical properties for the layers [24].

5. Conclusion

We have measured and analyzed the laser damage resistance of silica coatings made with different conventional deposition techniques. The thresholds are strongly dependent on the deposition technique and the test wavelength. At 1064 nm, the Dual Ion Beam Sputtering and Ion Assisted Electron Beam Deposition samples were found to have the better laser damage thresholds, and the Reactive Low Voltage Ion Plating and Ion Assisted Electron Beam Deposition samples were the more resistant at 355 nm. We have shown that the laser damage was initiated by different kinds of defects depending of the deposition technique and additional information (density, origin) about these defects have been obtained by a theoretical modeling of the laser damage probability curves.

We plan now to perform a similar study in the next months on single layers of a high index material (like HfO_2), then on optical interference filters combining these two materials.

References

- [1] D. Milam, W.H. Lowdermilk, F. Rainer, J.E. Swain, C.K. Carniglia, T.T. Hart, *Appl. Opt.* 21 (1982) 3689.
- [2] E. Hacker, H. Lauth, J. Meyer, P. Weissbrodt, R. Wolf, G. Zscherpe, H. Heyer, *Thin Solid Films* 192 (1990) 27.
- [3] P.F. Gu, J.F. Tang, *Opt. Lett.* 19 (1994) 81.
- [4] M. Alvisi, G. De Nunzio, M. Di Giulio, M.C. Ferrara, M.R. Perrone, L. Protopapa, L. Vasanelli, *Appl. Opt.* 38 (1999) 1237.
- [5] M. Alvisi, M. Di Giulio, S.G. Marrone, M.R. Perrone, L. Protopapa, A. Valentini, L. Vasanelli, *Thin Solid Films* 358 (2000) 250.
- [6] R. Thielsch, A. Gatto, J. Heber, N. Kaiser, *Thin Solid Films* 410 (2002) 86.
- [7] M.R. Kozlowski, in: F. Flory (Ed.), *Thin Films for Optical Systems*, Marcel Dekker, 1995, p. 521.
- [8] E. Hacker, H. Lauth, P. Weibrod, *Proc. SPIE* 2714 (1996) 317.
- [9] C.J. Stolz, F. Génin, in: N. Kaiser, H. Pulker (Eds.), *Optical Interference Coatings*, Springer, 2003, p. 309.
- [10] K.H. Guenther, T.W. Humpherys, J. Balmer, J.R. Bettis, E. Casparis, J. Ebert, M. Eichner, A.H. Guenther, E. Kiesel, R. Kuehnel, D. Milam, W. Ryseck, S.C. Seitel, A.F. Stewart, H. Weber, H.P. Weber, G.R. Wirtenson, R.M. Wood, *Appl. Opt.* 23 (1984) 3743.
- [11] M. Cathelinaud, F. Lemarquis, J. Loesel, B. Cousin, *Proc. SPIE* 5250 (2004) 511.
- [12] L. Gallais, J.Y. Natoli, *Appl. Opt.* 42 (2003) 960.
- [13] ISO 11254-1, *Determination of Laser-Damage Threshold of Optical Surfaces-Part 1: 1-on-1 Test.*, 2000.
- [14] H. Krol, L. Gallais, C. Grèzes-Besset, J.Y. Natoli, M. Commandré, *Opt. Commun.* 256 (2005) 184.
- [15] J. Dijon, T. Poiroux, C. Desrumaux, *Proc. SPIE* 2966 (1997) 315.
- [16] K. Yoshida, H. Yoshida, Y. Kato, C. Yamanaka, *J. Appl. Phys.* 47 (1985) 911.
- [17] J. Dijon, B. Rafin, C. Pellé, J. Hue, G. Ravel, B. André, *Proc. SPIE* 3902 (1999) 158.
- [18] Y. Xu, B. Zhang, W.H. Fan, D. Wu, Y. Han Sun, *Thin Solid Films* 440 (2003) 180.
- [19] K. Yoshida, T. Yabe, H. Yoshida, C. Yamanaka, *J. Appl. Phys.* 60 (1986) 1545.
- [20] S. Papernov, A.W. Schmid, *J. Appl. Phys.* 97 (2005) 114906.
- [21] A.H. Guenther, J.K. McIver, *Thin Solid Films* 163 (1988) 203.
- [22] L.J. Shaw-Klein, S.J. Burns, S.D. Jacobs, *Appl. Opt.* 32 (1993) 3925.
- [23] M. Alvisi, G. De Nunzio, M.R. Perrone, A. Rizzo, S. Scaglione, L. Vasanelli, *Thin Solid Films* 338 (1999) 269.
- [24] G.W. DeBell, *Proc. SPIE* 5991 (2005) 599116.